<u>REMARKS</u>

The withdrawal of the previous allowability of claims 1-11 by a Primary Examiner for the second time points up the great care this has required. *MPEP* 706.04.

The new rejection of claims 1-11 under 35 USC 103 for obviousness from the previously cited Chan patent and newly cited Chang and Farrens, et al. patents is traversed by the absence of rational underpinning to the three way combination.

> ... [R]ejections on obviousness cannot be sustained by mere conclusory statements; instead there must be some articulated reasoning with some rational underpinning to support the legal conclusion of obviousness. *Examination Guidelines for Determining Obviousness Under 35 U.S.C. 103 in View of the Supreme Court Decision in KSR International Co. v. Teleflex Inc.*, Fed. Reg. October 10, 2007, 57526, 57528-9.

The short answers why there is none are first that the Chang patent relates to vacuum bringing water boiling below the heating to 80°C, i.e., heating to 80°C or less, whereas the moderate temperatures claimed are 80°C or above.

PRIOR ART MUST BE CONSIDERED IN ITS ENTIRETY, INCLUDING DISCLOSURES THAT TEACH AWAY FROM THE CLAIMS *MPEP* 2141.02 VI (emphasis original)
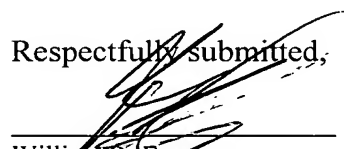
While it is true the temperature ranges touch, the teaching of the patent is reduction, whereas the claimed teaching is increase from the touch. (The rejection of claim 9 in this regard is, therefore, even more specifically wrong.)

The second short answer why the patents do not rationally underpin the rejection is that the Farrens, et al. patent, like the Chan patent, relates to plasma efforts from which one of ordinary skill in the art will recognize the impossibity of combination into the claimed invention from the Rieutord, et al. publication of record with the Information Disclosure Statement of November 16, 2006 (a further copy being attached for convenience).

Even if this were not the case, the Farrens, et al. patent does not disclose vacuum drying, as claimed, and, therefore, cannot disclose its combination with vacuum bonding or joining, as claimed. The Rarrens, et al. patent discloses at clo. 5, lines 27-28, "... other conventional ... drying technique ...," but such "other" is not an underpinning of the combination claimed.

Reconsideration and allowance are, therefore, requested.

Respectfully submitted,

William R. Evans
c/o Ladas & Parry LLP
26 West 61st Street
New York, New York 10023
Reg. No. 25858
Tel. No. (212) 708-1930

Dynamics of a Bonding Front

F. Rieutord,[1] B. Bataillou,[1,2,3] and H. Moriceau[2]

[1]CEA-Département de Recherche Fondamentale sur la Matière Condensée, F-38054 Grenoble Cedex 9, France
[2]CEA-Leti-Département des Technologies Silicium, F-38054 Grenoble Cedex 9, France
[3]Soitec, Parc Technologique des Fontaines, F-38190 Bernin, France
(Received 3 November 2004; published 13 June 2005)

A description of the bonding front propagation between two adhesive plates is proposed. The model relates the velocity of a bonding front to the adhesion energy, with application to wafer direct bonding. Its derivation is based on a competition between the bonding energy and the viscous drag of the air flow in the gap between the two wafers. The model describes well the experimental data, including the wafer deformation profile during bonding or the dependence of the velocity on the gas viscosity, pressure, and wafer thickness.

Adhesion processes are at play everywhere in our surroundings, from biological cell cohesion to tectonic plate motion, but remain poorly understood with regard to their physical or microscopic grounds. We address here the problem of the onset of adhesion between two solids through the dynamics of a bonding front. We used silicon wafers as an experimental model system, for their surfaces can be made clean and smooth enough to spontaneously adhere when brought together. This so-called wafer bonding process is generic, allowing one to assemble virtually any pair of materials regardless of their crystalline structure. Hence, it has found many industrial applications, one of the most important being the fabrication of silicon-on-insulator substrates by the bonding of oxide-covered silicon wafers [1]. When binding large silicon wafers, one can observe easily (e.g., using an infrared video camera) the bonding front propagation across the wafer assembly. This observation is often used as a quality control of the bonding process. However, no quantitative model for this process exists to date, although the influence of various parameters on the bonding front velocity have already been investigated in the literature [2–4]. The model we present here is inspired from those developed for drop spreading or dewetting dynamics [5–7].

It has been observed that the velocity of the bonding front is constant throughout the wafer. Writing the Navier-Stokes equation for the air flow between the two wafers, neglecting the inertial part (quasistatic regime), one gets

$$\frac{-1}{\rho}\frac{\partial p}{\partial x} + \frac{\eta}{\rho}\frac{\partial^2 v_x}{\partial y^2} = 0 \qquad (1)$$

where η and ρ are the viscosity and density of air. We assumed $\frac{\partial^2 v_x}{\partial x^2}$ is negligible as the flow is mainly oriented along x.

Solving this equation, a standard Poiseuille flow profile for the velocity is obtained

$$v_x = \frac{1}{2\eta}(y^2 - h^2)\frac{\partial p}{\partial x}.$$

$y = \pm h(x)$ are the equations for the boundary surfaces (Fig. 1). We assume here that the two wafers are identical and $h(x)$ is *half* the width of the air gap between the wafers. We have assumed here no-slip boundary conditions at the surfaces. Integrating this equation along y, one gets the flow rate Q through the cross section $S = 2hw$,

$$Q = -\frac{2h^3 w\rho}{3\eta}\frac{\partial p}{\partial x}$$

where h is the half height of the section and w its width.

Now, we define the propagating velocity of the bonding front U,

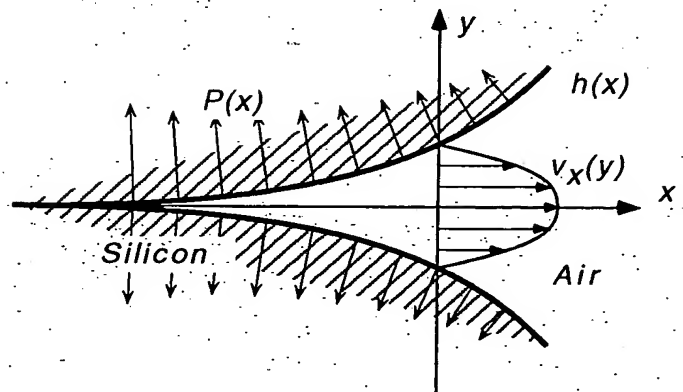$$U = \frac{-Q}{2hw\rho} = -\frac{h^2}{3\eta}\frac{\partial p}{\partial x}.$$

FIG. 1. Sketch showing the velocity profile of the air escaping the closing gap between the two deformed wafers [profile $h(x)$].

It is assumed here that the system is stationary, i.e., that at $t + dt$ the same system is just shifted by $U dt$. As a function of the constant velocity U, one can write

$$v_x = -\frac{3U}{2h^2}(y^2 - h^2).$$

Let us now write the power P_d dissipated in such a flow by viscous stress. It reads

$$P_d = \iiint \mathbf{F} \cdot \mathbf{v} \, dx \, dy \, dz = \iint -\frac{\partial p}{\partial x} v_x \, dS \, dx,$$

and, per unit length of the contact line,

$$P_d/w = \int_{x_{min}}^{x_{max}} \int_{-h(x)}^{h(x)} \eta \frac{3U}{2h^2} \frac{3U}{h^2}(y^2 - h^2) \, dx \, dy$$
$$= \int_{x_{min}}^{x_{max}} \eta \frac{6U^2}{h(x)} \, dx.$$

The lower boundary x_{min} is very important as the previous expression usually diverges for $h(x) \rightarrow 0$. In the following, the value of x_{min} will be taken such that $h(x_{min})$ corresponds to the molecular mean free path, as below this length scale the hydrodynamic viscous treatment is no longer valid in any case. The upper boundary x_{max} plays a much smaller role and its contribution can generally be neglected (taking $x_{max} = \infty$). This may not be the case however when the bonding wave comes close to the edge of the wafer, where the effects of a reduced dissipation produce an increase of the bonding velocity (which can be observed).

We write now the power of the driving force, i.e., the amount of energy obtained per time unit from the bonding forces (bf),

$$P_{bf} = 2\gamma w \frac{dx}{dt} = 2\gamma w U,$$

where 2γ is the bonding energy.

Equating these two power quantities, we obtain the equation giving the bonding front velocity

$$2\gamma w U = 6\eta U^2 w \int_{x_{min}}^{x_{max}} \frac{dx}{h(x)}$$

which yields

$$U = \frac{2\gamma}{6\eta \int_{x_{min}}^{x_{max}} \frac{dx}{h(x)}}. \tag{2}$$

Equation (2) is not in itself a direct relation between bonding velocity (U) and energy (2γ) as one needs to know the integral

$$\int_{x_{min}}^{x_{max}} \frac{dx}{h(x)}$$

for the considered profile. This profile depends on the bonding energy.

From an experimental point of view however, Eq. (2) is interesting as the velocity is usually measured from an IR video recording of the bonding front propagation. The video images do not only give positions of the bonding line, but also allow the reconstruction of the gap profile $h(x)$, through the observation of equal-thickness interference fringes (Fig. 2).

Interference fringes are seen on the pictures for an IR wavelength of $\lambda \approx 1.3 \, \mu$m i.e., showing contour lines every $\Delta 2h = \lambda/2 = 0.65 \, \mu$m. From the lateral spacing of these fringes, the profile can be reconstructed (see Fig. 3). The experimental profile can be used to estimate the dissipative part. Data are either fitted to the theoretical profile or integration is directly performed numerically. The most important part is the lower cutoff x_{min}. Taking x_{min} so that $2h_{min}$ is equal to the molecular mean free path Λ ($\Lambda = 0.5 \times 10^{-7}$ m for air at STP), we can calculate numerically the integral at the denominator of Eq. (2). For a bonding energy of $2\gamma = 100$ mJ/m^2, one would predict a velocity of the order of 2 cm/s, close to what is actually observed. We assume the air trapped between the two wafers has a viscosity at 20 °C of $\eta = 18.6 \times 10^{-6}$ Pa s.

We shall now determine the shape of the plate profiles when the bonding front advances (as measured using the IR interference fringes) and show that their deformation
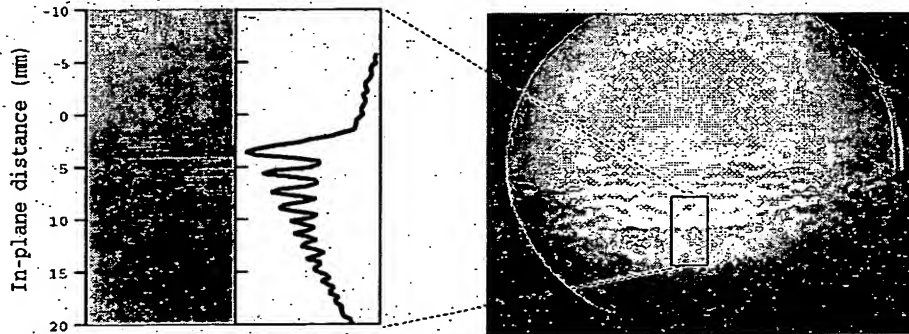

FIG. 2. IR photograph of the bonding front propagating across the wafer assembly. The video sequence allows the determination of the bonding velocity while the fringe pattern gives the wafer deformation profile close to the bonding line (see Fig. 3).
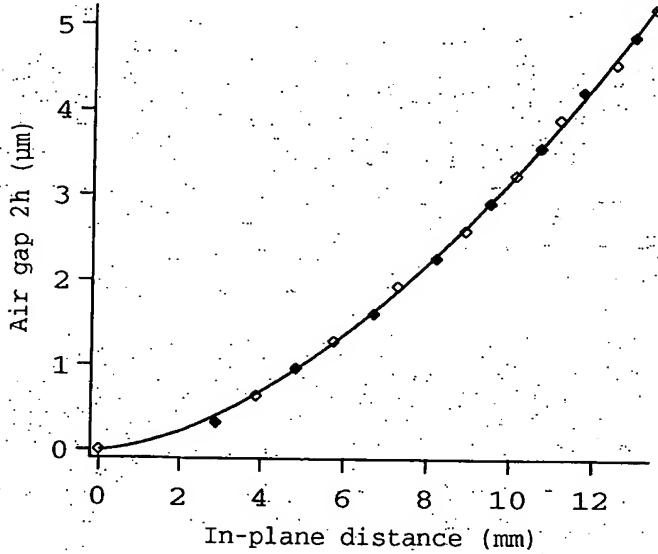
FIG. 3. Deformation profile of the wafers as measured from the equal-thickness interference fringes. Open and closed symbols correspond to the bright and dark fringes in Fig. 2. The solid line is a power law fit to the data giving exponent 1.65 ± 0.02, close to the predicted $5/3$.

(strain) is consistent with the pressure gradient that establishes during the bonding and which is responsible for the air outlet during the bonding phase.

Standard elasticity theory relates the plate deformation $h(x)$ to the stress (here the pressure exerted by the air inside the gap). This relation reads

$$\frac{Et^3}{12(1 - \nu^2)}\Delta^2 h - (P - P_0) = 0$$

(see, e.g., [8]). Here E is the Young's modulus, ν the Poisson ratio, and $P - P_0$ is the pressure difference between the inside of the wafer assembly and the outside.

The pressure P is obtained from its gradient and finally

$$D\frac{\partial^4 h}{\partial x^4} - \int_x^{x_{max}} \frac{3\eta U}{h^2(\xi)}d\xi = 0$$

where D is the bending rigidity of the plate ($D = \frac{Et^3}{12(1 - \nu^2)}$).

One has to find the profile $h(x)$ solution of this integro-differential equation.

Setting

$$l^2 = \frac{D}{3\eta U} = \frac{Et^3}{36(1 - \nu^2)\eta U}, \qquad (3)$$

l has the dimension of a length. Its order of magnitude using experimental data is 10^3 m. If one scales h and x to this length ($h_0 = h/l$, $u = x/l$), we obtain a dimensionless equation

$$\left(\frac{\partial^4 h_0}{\partial u^4}\right) - \int_u^\infty \frac{1}{h_0^2(\xi)}d\xi = 0.$$

When one looks for a power law solution $h_0(u) = Au^\alpha$, one finds a solution for

$$\alpha = 5/3$$

$$A^3 = \frac{1}{(2\alpha - 1)(\alpha - 3)(\alpha - 2)(\alpha - 1)\alpha} \Rightarrow A \approx 0.95.$$

The profile can then be written

$$h(x) = lh_0(x/l),$$

so that

$$h(x) = lA(x/l)^{5/3}. \qquad (4)$$

The Eq. (4) for the deformation predicts a profile that opens with the distance to the edge as a power $5/3$. Figure 3 shows the experimental profile as obtained from the equal-thickness interference fringes. It can be seen that there is a good agreement between the data and the model. From the fit to the data, the profile parameter length l can be measured ($l = 3000$ m).

Replacing this expression for $h(x)$ in the integral of Eq. (2), one obtains the expression for U:

$$U = \frac{\gamma}{3\eta \int_{x_{min}}^{x_{max}} \frac{dx}{h(x)}} = \frac{2\gamma}{9\eta}A\left(\frac{x_{min}}{l}\right)^{2/3} = \frac{2\gamma}{9\eta}A^{3/5}\left(\frac{h_{min}}{l}\right)^{2/5}$$

The integration limit x_{min} is taken such that $2h_{min}$ equals the mean free path Λ and x_{max} is set to infinity. With the previous value for l, we obtain $U = 2$ cm/s for $2\gamma = 0.1$ J/m², in agreement with the observed velocity.

Combining with expression (3) for l, we obtain an expression for the velocity U of the bonding front:

$$U = \frac{(2\gamma)^{5/4}}{\eta t^{3/4}}\frac{\Lambda^{1/2}}{(\frac{E}{1 - \nu^2})^{1/4}}(1/9A^{3/4}). \qquad (5)$$

Again, taking standard parameter values, $E = 130$ GPa, $\nu = 0.29$, $\Lambda = 0.5 \times 10^{-7}$ m, $\eta = 18.6 \times 10^{-6}$ Pa s, and $t = 525$ μm, we find a velocity of the order of 2 cm/s for $2\gamma = 0.1$ J/m².

Formula (5) predicts a decrease of bonding velocity with wafer thickness: thicker wafers will deform less, thus forcing the air to escape through a closer wedge with increased dissipation. More precisely, Eq. (5) predicts

$$U \propto \frac{1}{t^{3/4}}.$$

The dependence was investigated by Gösele [2] and Bengtsson [4] experimentally. Gösele found no dependence with thickness while Bengtsson et al. did observe a decrease of the bonding velocity. They proposed a dependence as $-t^{3/2}$. Other experiments also found a decrease in velocity when one or both wafers were attached to a rigid block at their back [9], but here a linear decrease of the

velocity with thickness was proposed. We performed experiments on both 4″ ($t = 525$ μm) and 8″ wafers ($t = 725$ μm). A velocity ratio of 1.31 was found in good agreement with the $t^{-3/4}$ ratio (1.27).

A study of bonding velocity as a function of gas viscosity has been performed by Tong and Gösele [10]. When plotted as a function of the inverse viscosity, the bonding velocity gives a straight line in agreement with the previous expression. Quantitatively, they obtained a slope of 0.44×10^{-6} N/m. Calculating the product $U\eta$ using the measured experimental profile, one gets 0.47×10^{-6} N/m, in fair agreement [11].

The dependence with air pressure can also be checked using Eq. (5). The viscosity of a gas does not depend on pressure, so that the only dependence with pressure P that appears in Eq. (5) is through the molecular mean free path Λ:

$$\Lambda = \frac{1}{N\sigma} = \frac{RT}{P\sigma},$$

where N is the number of molecules per unit volume, σ their cross section, and R the gas constant. Thus we predict that the bonding speed should decrease with pressure as $P^{-1/2}$. This study was performed by Gösele *et al.* [2] and the $P^{-1/2}$ variation was observed. Here again the data are consistent with our model. Note, however, that when pressure P decreases, other terms may change in the formula as this may induce desorption of adsorbed species (e.g., water) so that 2γ will change. Indeed, the $P^{-1/2}$ function reproduces the hydrophobic bonding behavior better. Also, at very low pressures, when the whole system is in the Knudsen regime, our approximate treatment will not be adequate and more realistic assumptions will be needed. *A fortiori*, for ultrahigh vacuum bonding, gas flow dissipation is absent resulting in much higher bonding velocities that can only be explained using terms neglected in the present description (e.g., wafers inertia).

Finally, we find that the bonding front velocity should depend on the power 5/4 of the bonding energy. Such a dependence would be worth checking although due to the difficulty of measuring E accurately, the exact value of the exponent in the power law dependence is not easy to determine. A linear dependence has been reported [9], but the data accuracy makes these data also compatible with our 5/4 exponent.

Note that we have assumed in our treatment that no large changes of elastic energy were occurring during the bond wave propagation. This is backed by the observation of a translational invariance of the deformation profile, at least when the bond wave is not close to the wafer edge.

In conclusion, we propose a quantitative description of the dynamics of the adhesion process. Our model is consistent with the measurements and other data available from the literature. Hence, the bonding front velocity measurement can be proposed as a method to determine the bonding energy in a quantitative and nondestructive way. Equations (2) or (5) can be used for that purpose. At the moment, the full validation of these calculations, e.g., a precise study of the bonding velocity with different adhesion energies, is limited by the accuracy of the independent measurement of the bonding energy (using, e.g., the crack-opening method). Note also that the measurements have to be performed in the same conditions as the bonding experiment and possibly at the same time, e.g., by propagating the bonding front against a spacer. Time dependence of the bonding energy has been reported with rather fast aging kinetics at short times.

[1] M. Bruel, Electron. Lett. **31**, 1201 (1995).
[2] U. Gösele, S. Hopfe, S. Li, S. Mack, T. Martini, M. Reiche, E. Schmidt, H. Stenzel, and Q.-Y. Tong, Appl. Phys. Lett. **67**, 863 (1995).
[3] Q.-Y. Tong and U. Gösele, *Semiconductor Wafer Bonding: Science and Technology* (John Wiley & Sons, New York, 1999).
[4] S. Bengtsson, K. Ljungberg, and J. Vedde, Appl. Phys. Lett. **69**, 3381 (1996).
[5] P.-G. de Gennes, Rev. Mod. Phys. **57**, 827 (1985).
[6] P. Martin and F. Brochard-Wyart, Phys. Rev. Lett. **80**, 3296 (1998).
[7] F. Rieutord, O. Rayssac, and H. Moriceau, Phys. Rev. E **62**, 6861 (2000).
[8] L. Landau and E. Lifshitz, *Théorie de l'elasticité* (Editions Mir, Moscow, 1967).
[9] G. A. C. M. Spierings, J. Haisma, and T. M. Michielsen, Philips J. Res. **49**, 47 (1995).
[10] Q.-Y. Tong and U. Gösele, in Ref. [3], Fig. 4.23, p. 78.
[11] The viscosity point for Argon seems to be misplaced on the curve of Ref. [10] so that the linear behavior may be less accurate. This is not unexpected as changing the gas also alters the mean free path value Λ.